JOURNAL OF GEOPHYSICAL RESEARCH: ATMOSPHERES, VOL. 118, 4657–4669, doi:10.1002/jgrd.50411, 2013

The role of circulation features on black carbon transport into the Arctic in the Community Atmosphere Model version 5 (CAM5)

Po-Lun Ma,[1] Philip J. Rasch,[1] Hailong Wang,[1] Kai Zhang,[1] Richard C. Easter,[1] Simone Tilmes,[2] Jerome D. Fast,[1] Xiaohong Liu,[1] Jin-Ho Yoon,[1] and Jean-Francois Lamarque[2]

Received 4 January 2013; revised 9 April 2013; accepted 11 April 2013; published 28 May 2013.

[1] Current climate models generally underpredict the surface concentration of black carbon (BC) in the Arctic due to the uncertainties associated with emissions, transport, and removal. This bias is also present in the Community Atmosphere Model version 5.1 (CAM5). In this study, we investigate the uncertainty of Arctic BC due to transport processes simulated by CAM5 by configuring the model to run in an "off-line mode" in which the large-scale circulation features are prescribed. We compare the simulated BC transport when the off-line model is driven by the meteorology predicted by the standard free-running CAM5 with simulations where the meteorology is constrained to agree with reanalysis products. Some circulation biases are apparent: the free-running CAM5 produces about 50% less transient eddy transport of BC than the reanalysis-driven simulations, which may be attributed to the coarse model resolution insufficient to represent eddies. Our analysis shows that the free-running CAM5 reasonably captures the essence of the Arctic Oscillation (AO), but some discernable differences in the spatial pattern of the AO between the free-running CAM5 and the reanalysis-driven simulations result in significantly different AO modulation of BC transport over northeast Asia and eastern Europe. Nevertheless, we find that the overall climatological circulation patterns simulated by the free-running CAM5 generally resemble those from the reanalysis products, and BC transport is very similar in both simulation sets. Therefore, the simulated circulation features regulating the long-range BC transport are unlikely the most important cause of the large underprediction of surface BC concentration in the Arctic.

Citation: Ma, P.-L., P. J. Rasch, H. Wang, K. Zhang, R. C. Easter, S. Tilmes, J. D. Fast, X. Liu, J.-H. Yoon, and J.-F. Lamarque (2013), The role of circulation features on black carbon transport into the Arctic in the Community Atmosphere Model version 5 (CAM5), *J. Geophys. Res. Atmos.*, *118*, 4657–4669, doi:10.1002/jgrd.50411.

1. Introduction

[2] Aerosols containing black carbon (BC) can exert a significant forcing globally [*Bond et al.*, 2013] and in the Arctic, on the atmosphere, and on snow and ice at the surface owing to its strong radiative absorption [*Flanner et al.*, 2007, 2009; *Hansen and Nazarenko*, 2004], altering both regional and global climate. Current general circulation models (GCMs), including the Community Atmosphere Model (CAM), show only limited skills in simulating the distribution of aerosols [*Lee et al.*, 2012; *Textor et al.*, 2006], and models agree more with the observations near source regions and less at remote areas [*Lee et al.*, 2012; *Rasch et al.*, 2000]. Most models greatly underpredict BC concentration in the Arctic, especially the surface concentration in wintertime [*Koch et al.*, 2009; *Shindell et al.*, 2008], during the Arctic haze season [*Law and Stohl*, 2007; *Quinn et al.*, 2007], and overestimate BC concentrations aloft [*Schwarz et al.*, 2010]. These biases may arise from deficiencies in model representations of aerosol's emission, transport, or removal processes.

[3] In this paper, we explore some of the reasons for biases in CAM version 5.1 (CAM5) [*Neale et al.*, 2010] (P.J. Rasch, et al. The Community Atmosphere Model Version 5 (CAM5), in preparation, 2013) simulations. A number of recent studies [*Liu et al.*, 2011, 2012; *Wang et al.*, 2013, 2011a] have suggested that the discrepancy between simulated and the observed Arctic BC concentrations could be substantially reduced by improving the model's treatment of BC aging, cloud processes, and subgrid scale convective transport and turbulent mixing at lower latitudes (the bias is not solely attributable to processes in the Arctic), since the aerosols available for transport by the winds in GCMs are closely coupled to these processes. In a companion paper

[1]Atmospheric Sciences and Global Change Division, Pacific Northwest National Laboratory, Richland, Washington, USA.
[2]Atmospheric Chemistry Division, National Center for Atmospheric Research, Boulder, Colorado, USA.

Corresponding author: P.-L. Ma, Atmospheric Sciences and Global Change Division, Pacific Northwest National Laboratory, Richland, WA, USA. (Po-Lun.Ma@pnnl.gov)

2169-897X/13/10.1002/jgrd.50411

Table 1. Brief Description of the Model Configurations

Experiment	Description
CAM5_AMIP_ORI	Standard CAM5.1
	Dust emission factor = 0.35
	Sea salt emission factor = 1.35
CAM5_AMIP	Off-line mode driven by CAM5_AMIP_ORI
	Dust emission factor = 0.68
	Sea salt emission factor = 1.05
CAM5_ERAI	Off-line mode driven by ERA-Interim
	Surface moisture flux factor = 0.86
	Dust emission factor = 1.66
	Sea salt emission factor = 1.23
CAM5_MERRA	Off-line mode driven by MERRA
	Surface moisture flux factor = 0.86
	Dust emission factor = 1.78
	Sea salt emission factor = 1.05

[*Wang et al*., 2013], we explore the simulation sensitivity to these processes in CAM5 and describe a set of modifications to process representations that improve the fidelity of the simulation substantially in terms of the magnitude and seasonal variation of BC concentrations in CAM5, as well as the vertical profile of BC at high latitudes. However, a variety of biases shared by other transport and climate models are still present, suggesting that either the model deficiencies in representing BC emissions and removal are not fully addressed, or the simulated circulation features are biased low in poleward transport of energy and tracers. The uncertainty of the emission inventory, generally considered to be at least a factor of 2 [*Bond et al*., 2004; *Ramanathan and Carmichael*, 2008], may also contribute to the model bias. For example, using a reanalysis data set to drive the global chemical transport mode, *Wang et al*. [2011b] found that doubling BC emissions in Asia and Russia is essential to improve the agreement between the model and the observations in the Arctic.

[4] In this study, we explore the possibility that some of the remaining spatial and temporal biases in BC distributions may be due to the transport processes that carry BC from sources at lower latitudes to the Arctic [*Fisher et al*., 2010; *Huang et al*., 2010; *Koch and Hansen*, 2005; *Stohl*, 2006]. Our goal is to understand the role of circulation features generally resolved by GCMs on BC transport into the Arctic (defined in this study as the area poleward of 66.5°N), and investigate how much of the remaining biases in Arctic BC can be explained by the circulation biases. We use simulations with CAM5, evaluating the model-simulated BC transport produced with the model's standard configuration ("free-running mode") where the model meteorology evolves according to its internal physical representations, to simulations where the model's meteorology is constrained to agree with reanalysis products. The model is described in section 2. In section 3, we discuss the simulated poleward BC transport and its physical mechanisms, as well as modulation of BC transport associated with important circulation features. Conclusions are drawn in section 4.

2. Model Configuration and Experimental Design

[5] Our simulations use various configurations of CAM5, the atmospheric component of the Community Earth System Model (CESM) version 1.0.3. In addition to run CAM5 in the standard "free-running" mode, we have configured the model to operate in an "off-line" mode. In the free-running mode, model fields (temperature, winds, surface pressure, stress, heat, and moisture flux) are allowed to evolve according to the model's governing equations, and fields respond to climatic forcing agents such as greenhouse gases, aerosol, and prescribed sea surface temperature (SST). In the off-line mode, the model reads in the archived meteorological fields (wind and temperature profiles, and surface pressure, stress, heat flux, and moisture flux) every 6 h, and the model-predicted fields are overwritten by interpolating adjacent 6 h off-line data at each time step. The CAM5 physical and chemical parameterizations calculate the evolution of aerosol, water (vapor and condensate), cloud amount, convective transport, precipitation, etc., based on the prescribed meteorological fields. Off-line models are used routinely for studying atmospheric transport issues [*Bey et al*., 2001; *Chin et al*., 2000; *Chipperfield*, 2006; *Emmons et al*., 2010; *Ginoux et al*., 2001; *Heimann*, 1995; *Jacob et al*., 1997; *Lamarque et al*., 2012; *Lawrence et al*., 1999; *Rasch et al*., 1997; *von Kuhlmann et al*., 2003a, 2003b]. This study is the first to use CAM with the CAM5 physics suite as an off-line model. The methodology follows closely that developed for CAM with Chemistry (CAM-Chem) [*Lamarque et al*., 2012]. While the CAM-Chem model uses the CAM version 4 (CAM4) physics suite and the bulk aerosol parameterizations from the Model for OZone And Related chemical Tracers (MOZART) chemistry package [*Emmons et al*., 2010], we use the very different CAM5 suite that includes the 3-mode Modal Aerosol Model (MAM3) [*Liu et al*., 2012] to simulate the water and the aerosol lifecycle in this study. The free-running simulation uses the standard CAM5 physics suite, while the off-line simulations adopt the revised physical parameterization package as described below. Preliminary experiments (not shown) indicate that off-line CAM5 simulations using archived CAM5 fields are virtually identical to their free-running counterparts (as they should be), when the same physics suite is used in both simulations.

[6] Both *Wang et al*. [2011a] and *Liu et al*. [2012] showed that CAM5 removes aerosols very aggressively when they are transported from low- and midlatitude source regions to high latitudes. The wet-removal bias in the model produces surface aerosol mixing ratios in the Arctic that are 2–3 orders of magnitude lower than observed values with seasonal variations that do not resemble the observations. CAM5 aerosol wet removal includes both in-cloud and below-cloud scavenging processes. The in-cloud scavenging consists of two steps: activation that converts the interstitial aerosols to cloud-borne aerosols, and precipitation that removes the cloud-borne aerosols. The below-cloud scavenging process removes aerosol particles through impaction of raindrops and snow [*Liu et al*., 2012]. In *Wang et al*. [2013], we demonstrated that dramatic improvements in arctic surface BC concentration and the vertical profile could be achieved by a reformulation of the aerosol convective transport and liquid cloud wet-removal parameterizations. The revised physics package (labeled as ALL_m3 in *Wang et al*. [2013]) is used in the three off-line simulations in this study. The revised physics package includes (1) the elimination of minor inconsistencies in the treatment of liquid clouds, (2) a unified treatment of aerosol convective transport and wet scavenging associated with convective clouds,

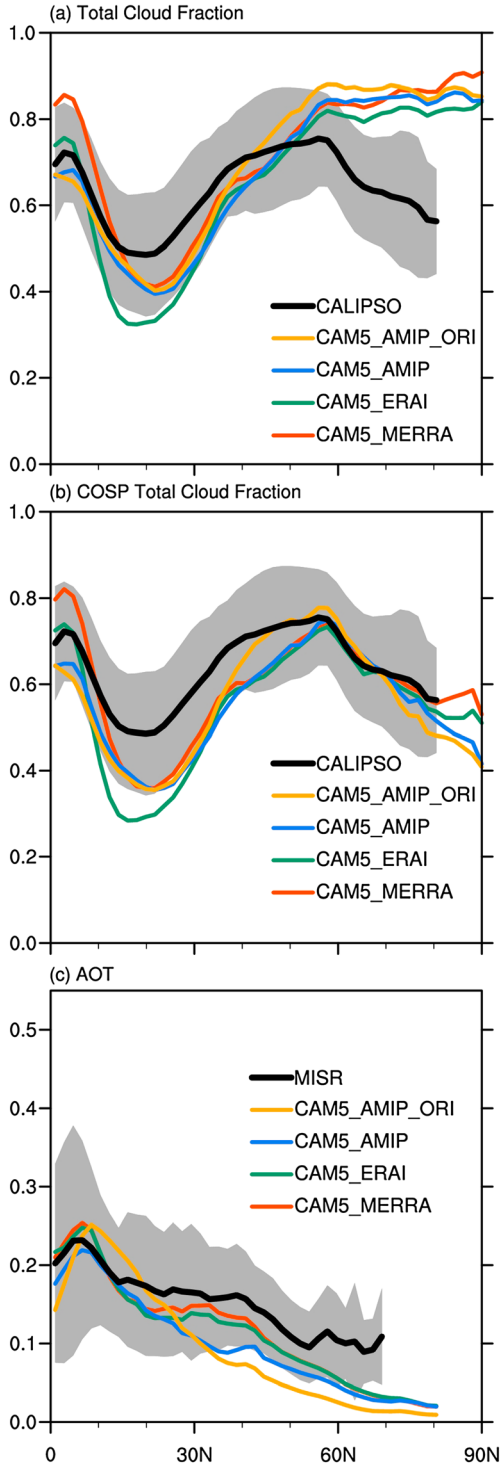

Figure 1. Wintertime zonal average (a) total cloud fraction from 2006 to 2010, (b) COSP-simulated total cloud fraction from 2006 to 2010, and (c) AOT from 2001 to 2010. Model results are evaluated against satellite observation (CALIPSO for total cloud fraction; MISR for AOT). Shaded area represents spatial variability of the observation ranges within one standard deviation from the mean.

(3) a 40% lower hygroscopicity of aerosols, and (4) a reduction of the liquid cloud fraction in supercooled liquid clouds [*Vavrus and Waliser*, 2008].

[7] The model is configured with a horizontal grid spacing of 1.9° by 2.5°. Four 22 year model simulations (Table 1) from 1989 to 2010 were performed. The anthropogenic emissions in this period are taken from IPCC AR5 emission data set [*Lamarque et al*., 2010]. The model was first run for a year for spin-up, and the output at the last time step from the spin-up run was then used as the initial condition for the following experiments.

[8] The first experiment (listed as CAM5_AMIP_ORI) adopts the standard free-running CAM5 settings with 30 vertical levels in accordance with the Atmospheric Model Intercomparison Project (AMIP) protocol in which CAM5 is constrained by realistic SST and sea ice, and all the atmospheric processes are computed within the model [*Gates et al*., 1999]. The remaining three experiments are configured in off-line mode with the same horizontal grid spacing as the free-running CAM5 but with 56 hybrid pressure-sigma levels in the vertical. The vertical levels are defined to match the bottom 56 levels used in NASA's Goddard Earth Observing System Data Assimilation System version 5 (GEOS-5) that generates Modern Era Retrospective-Analysis for Research and Applications (MERRA) reanalysis data set [*Rienecker et al*., 2011], and meteorological fields from the reanalysis products (0.7° by 0.7° for ERA-Interim [*Dee et al*., 2011] and 0.47° by 0.53° for MERRA) are interpolated in the horizontal to match CAM5's grid spacing of 1.9° by 2.5°.

[9] The second experiment is run in the off-line mode using meteorology archived from the CAM5_AMIP_ORI simulation but with revised physics package in *Wang et al*. [2013] to investigate aerosol transport in the model with improved parameterization without allowing the change of aerosol forcing to affect the meteorology. Experiments three and four, listed as CAM5_ERAI and CAM5_MERRA, are driven by two modern reanalysis products, ERA-Interim [*Dee et al*., 2011] and MERRA [*Rienecker et al*., 2011], respectively. In this study, our focus is on the similarities and differences between the GCM-driven (CAM5_AMIP) and reanalysis-driven (CAM5_ERAI and CAM5_MERRA) simulations.

[10] For these two reanalysis-driven off-line experiments, we have introduced a tunable scale factor to decrease surface moisture flux. This tunable parameter is set to 0.84 (effectively decreasing the flux to 84% of that provided by the reanalysis products) based on a pair of previous simulations that contrast the surface moisture flux archived in ERA-Interim and calculated in CAM5 when the meteorology is constrained by ERA-Interim. In other words, we use the spatial distribution and temporal evolution of the surface moisture flux as archived in ERA-Interim, but set the magnitude to produce a globally averaged value similar to that computed by the standard CAM5 given the meteorology of ERA-Interim. The scale factor is chosen so that the low-level liquid cloud amount in reanalysis-driven simulations is similar to that in the free-running CAM5. The same scale factor is also applied in CAM5_MERRA. This setting is essential to keep the in-cloud wet scavenging of aerosols, which dominates the scavenging process in CAM5 [*Wang et al*., 2013], at a similar magnitude in different model configurations.

[11] In CAM5, the natural aerosols (sea salt and mineral dust) can affect the BC and water substances (vapor and clouds) by altering the aerosol size distribution and hygroscopicity, and

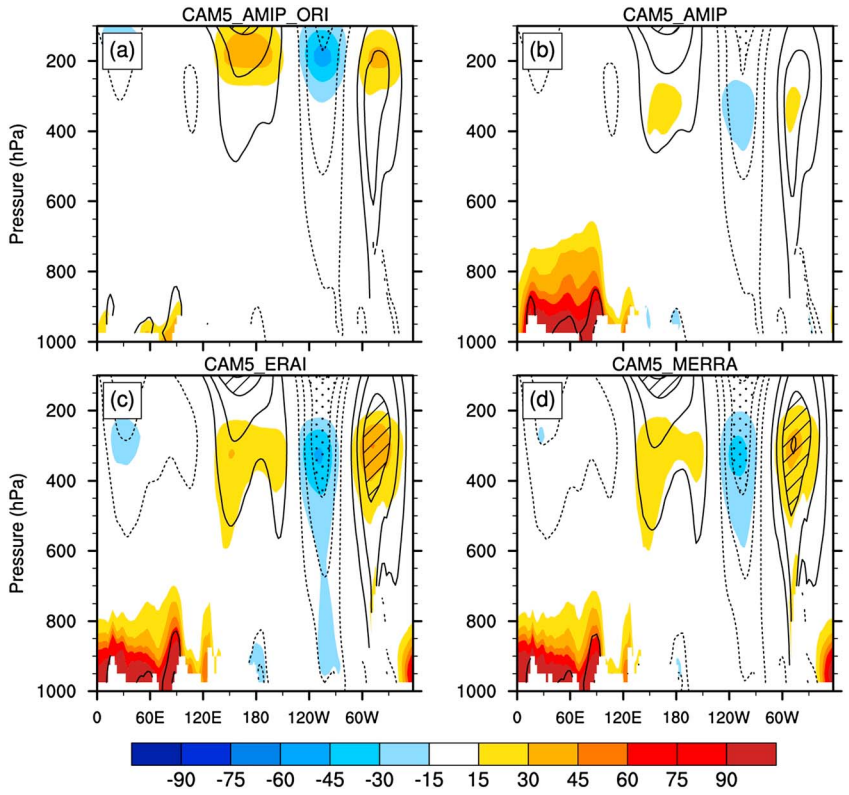

Figure 2. Cross-section (at 66.5°N) of meridional BC flux (color shaded; unit = ng s^{-1} m^{-2}) and meridional wind (black contours with interval = 3 m s^{-1}) averaged over 22 years of DJF. Strong (wind speed 3 m s^{-1}) poleward (equatorward) winds are enclosed by solid (dotted) contours. Areas with meridional winds higher (lower) than 9 m s^{-1} (−9 m s^{-1}) are denoted by stripes (dots).

eventually the wet removal of BC [*Liu et al*., 2012]. Hence, in order to keep the annual average global sea salt and dust mobilization from all experiments about the same, and to keep the annual average global aerosol optical thickness (AOT) about 0.135, we tune the exogenous parameters, the surface mobilization coefficients (i.e., the "emission" scale factors) for sea salt and dust, in the off-line experiments to account for the fact that the surface wind stress in the free-running CAM5, ERA-Interim, and MERRA is different. To perform a fair comparison of the aerosol transport process between different model configurations, we keep all the tunable parameters in cloud microphysics and macrophysics, deep and shallow convections, turbulence, and aerosol parameterizations identical. The configuration of each experiment is summarized in Table 1.

3. Results

3.1. Distribution of Clouds and Aerosols

[12] Cloud amount and distribution directly affect the aerosol wet-scavenging and thus aerosol distributions. Hence, we first evaluate the simulated clouds in different model configurations. Because the Cloud-Aerosol Lidar and Infrared Pathfinder Satellite (CALIPSO) is able to detect clouds that are thin or over bright surface [*Kay et al*., 2012], providing reliable cloud estimates in the polar region, we use CALIPSO estimates for boreal winter (December-January-February (DJF)) from 2006 to 2010, obtained from the Cloud Feedbacks Model Intercomparison Project (CFMIP) [*Bony et al*., 2011], to evaluate model simulations. Figure 1a shows that the model-calculated mid- and high-latitude raw cloud fraction is much higher than CALIPSO since model cloud fraction can produce clouds below the detection limit of CALIPSO. Comparisons using the CFMIP Observation Simulator Package (COSP) in CAM5 [*Chepfer et al*., 2008, 2010; *Kay et al*., 2012] that estimate clouds as the satellite would see them agree closely, especially in the high latitudes (Figure 1b). Between 40°N and 70°N, CAM5_AMIP_ORI shows much higher cloud fraction than the three off-line experiments that run with the *Wang et al*. [2013] revised physics package. Since the anthropogenic emissions are concentrated in the low and middle latitudes, the larger cloud fraction in the region in the standard CAM5 can lead to unrealistically strong wet removal of the aerosols.

Table 2. Net Meridional BC Flux (Unit = μg s^{-1} m^{-1}) Across 66.5°N in DJF, Averaged Over 22 Years

	CAM5_AMIP_ORI	CAM5_AMIP	CAM5_ERAI	CAM5_MERRA
Total BC flux	10.4	50.3	56.5	58.7
Above 700 hPa	3.3	4.8	6.5	7.2
Below 700 hPa	7.1	45.5	50	51.5

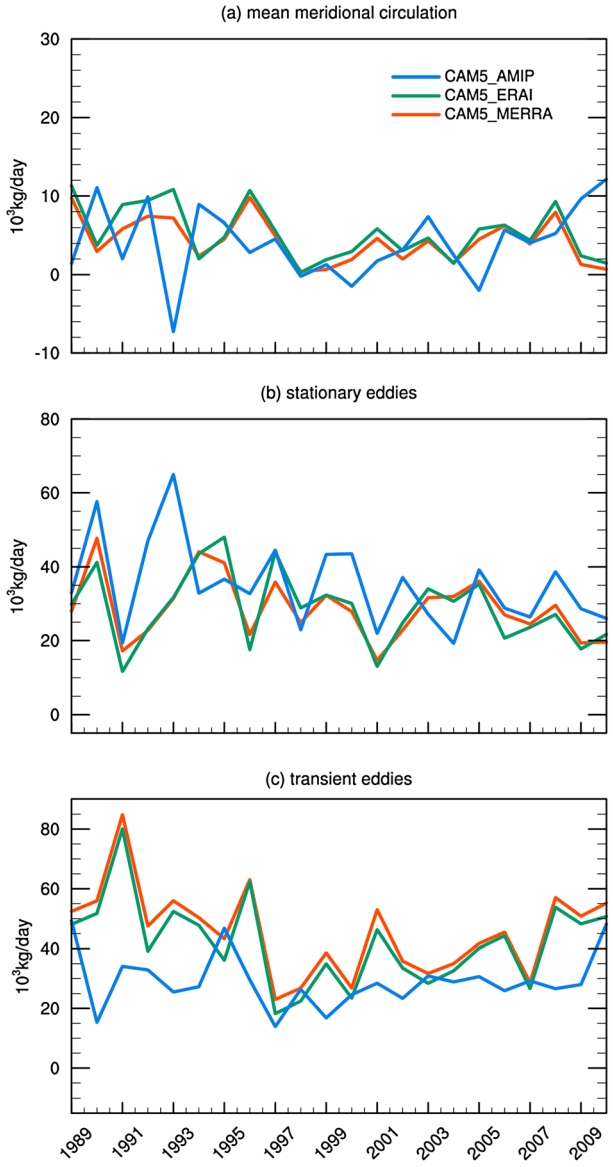

Figure 3. Time series of meridional BC flux (unit = 10^3 kg day^{-1}) at 66.5°N in DJF by (a) mean circulation, (b) stationary eddies, and (c) transient eddies.

In Figure 1c, level 3 monthly average AOT from the multiangle imaging spectroradiometer (MISR) [*Kahn et al.*, 2010] for all winter months in 2001–2010 is used to evaluate model simulations. MISR AOT is in good agreement with ground-based observations except for extreme conditions such as when AOT is larger than 0.4 or smaller than 0.02 [*Kahn et al.*, 2010]. The results show that model simulations agree with the observations in the low latitudes (south of 30°N), but all model simulations underestimate AOT significantly north of 60°N, which may be due to the model deficiencies in transport, emissions, and cloud processes. Further model evaluation is given in Appendix A.

3.2. Poleward BC Transport

[13] The 22 year mean meridional BC flux driven by the GCM-simulated circulation appears to have similar pathways (Figure 2) and magnitude (Table 2) when compared with the reanalysis-driven simulations. In the lower troposphere, a large poleward BC flux is observed near northern Europe, extended from 30°W to 120°E for CAM5_ERAI and CAM5_MERRA (Figures 2c and 2d) but shifted eastward by about 30°, from 0°E to 120°E for CAM5_AMIP (Figure 2b) due to stronger westerlies over North Atlantic and Europe in the GCM-driven simulation that moves BC eastward (figure not shown). In this region, the meridional BC flux extends to higher altitudes (about 700 hPa) when driven by the free-running CAM5 than the reanalysis products (about 800 hPa) due to stronger convective transport in the lower troposphere (indicated by diagnosed convective mass flux; not shown). The lower tropospheric BC flux is significantly increased while using the revised parameterization package (CAM5_AMIP) compared with the simulation using the original model parameterization package (CAM5_AMIP_ORI)

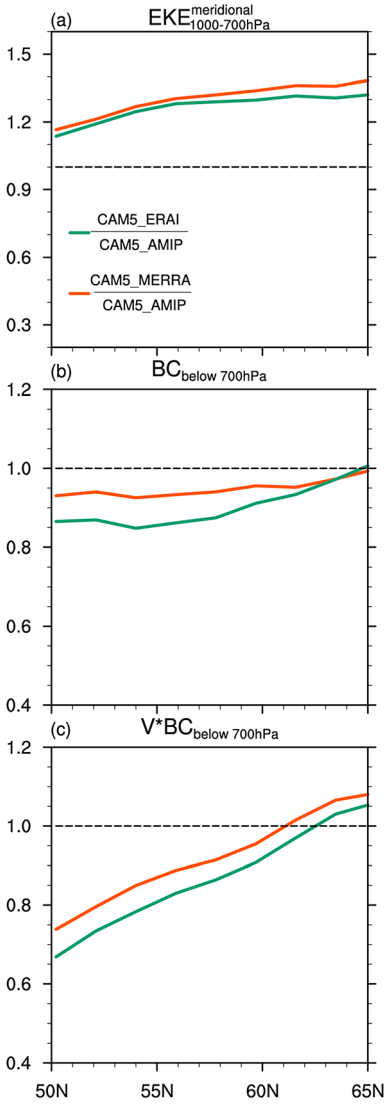

Figure 4. Lower tropospheric (a) eddy kinetic energy, (b) BC burden, and (c) meridional BC flux of the reanalysis-driven simulations in DJF as a function of latitude, averaged over eastern Atlantic/northern Europe region (30°W–90°E) and normalized with respect to the GCM-driven simulation. Dashed line represents the 1:1 ratio.

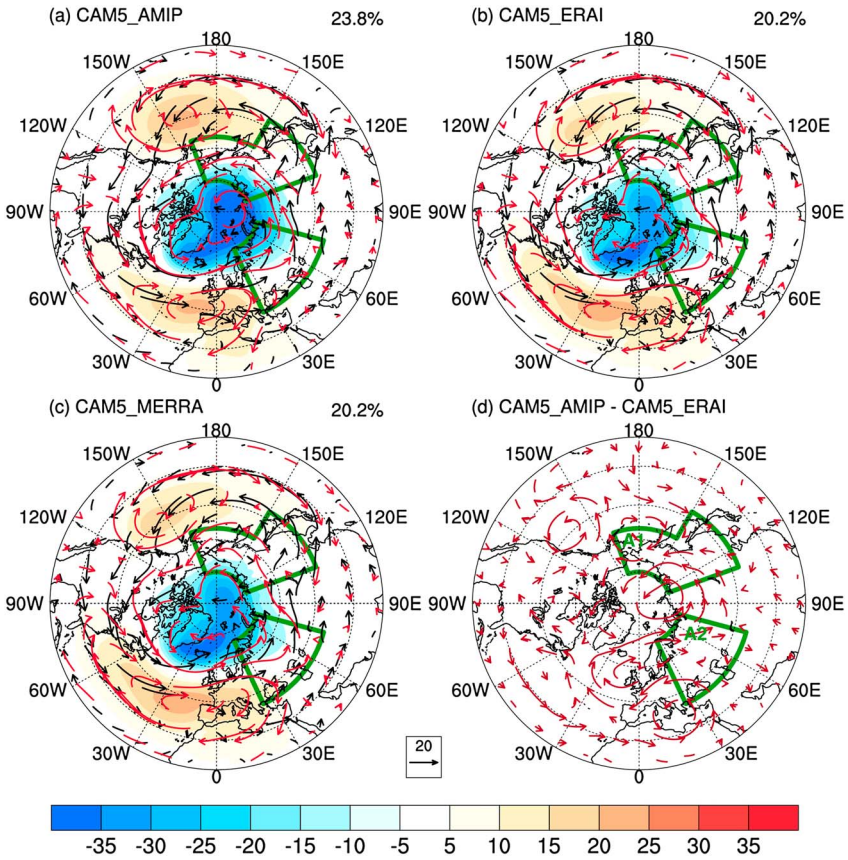

Figure 5. Leading EOF shown as the regression map of 1000 hPa geopotential height (color shaded; unit: m), 22 year DJF mean lower tropospheric (below 688 hPa) air mass flux (black vectors; unit: 10^3 kg m^{-1} s^{-1}), and lower tropospheric air mass flux (red vectors; unit: 10^2 kg m^{-1} s^{-1}) regressed onto the AO index simulated by (a) CAM5_AMIP, (b) CAM5_ERAI, and (c) CAM5_MERRA, and (d) the difference of the regressed lower tropospheric air mass flux (red vectors; unit: 10^2 kg m^{-1} s^{-1}) between CAM5_AMIP and CAM5_ERAI. Explained variance of the EOF is shown at upper-right corner of each panel. Two areas of interest are marked as A1 and A2.

due to much higher tropospheric BC burdens associated with weaker wet removal in CAM5_AMIP.

[14] In the upper troposphere, the meridional BC flux at 66.5°N appears to follow the winds associated with planetary waves, and the northward and southward BC flux largely offset each other. The two reanalysis-driven experiments produce much stronger (about 60%) meridional winds than the GCM-driven simulation (CAM5_AMIP). Upper tropospheric BC concentration over the Pacific sector (120°E to 30°W) is about 10–20% higher than the GCM-driven simulation due to lower cloud amounts in the reanalysis-driven simulations. As a result, stronger upper tropospheric meridional BC flux is observed in the reanalysis-driven simulations over this area.

[15] Previous studies suggest that the poleward BC transport in the lower troposphere over northern Europe is the most efficient transport pathway of BC into the Arctic [*Stohl*, 2006]. Despite the fact that all model configurations are able to capture this feature, the lower tropospheric poleward BC flux in this region in the GCM-driven simulation is significantly weaker than the reanalysis-driven simulations. To understand the mechanisms driving the difference, the total meridional BC flux below 700 hPa across 66.5°N is decomposed into fluxes associated with the mean meridional circulation, the stationary eddies, and the transient eddies, respectively:

$$[\overline{VQ}] = [\bar{V}][\bar{Q}] + [\overline{V^*}\ \overline{Q^*}] + \left[\overline{V'Q'}\right];$$

where V is the meridional wind speed and Q is the BC mixing ratio; the time average, zonal average, deviation from the time average, and deviation from the zonal average are denoted by overbar ($\bar{}$), bracket ([ ]), prime ($'$), and asterisk(*), respectively. The results are depicted in Figure 3.

[16] In this analysis, the 22 year mean meridional BC flux at 66.5°N and the associated standard deviation by the mean meridional circulation in CAM5_AMIP, CAM5_ERAI, and CAM5_MEERA experiments are 4.0 ± 4.7, 5.3 ± 3.4, and 4.3 ± 2.9 (10^3 kg day^{-1}), respectively; by stationary eddies, 35.1 ± 11.8, 28.7 ± 9.9, and 28.7 ± 8.6 (10^3 kg day^{-1}), respectively; and by transient eddies, 29.2 ± 9.2, 41.9 ± 14.4, and 45.6 ± 14.5 (10^3 kg day^{-1}), respectively. As shown in Figure 3, the two reanalysis-driven simulations yield very similar results. The eddy transport term dominates total poleward BC flux at this latitude. Moreover, these two simulations show a significantly larger transient eddy

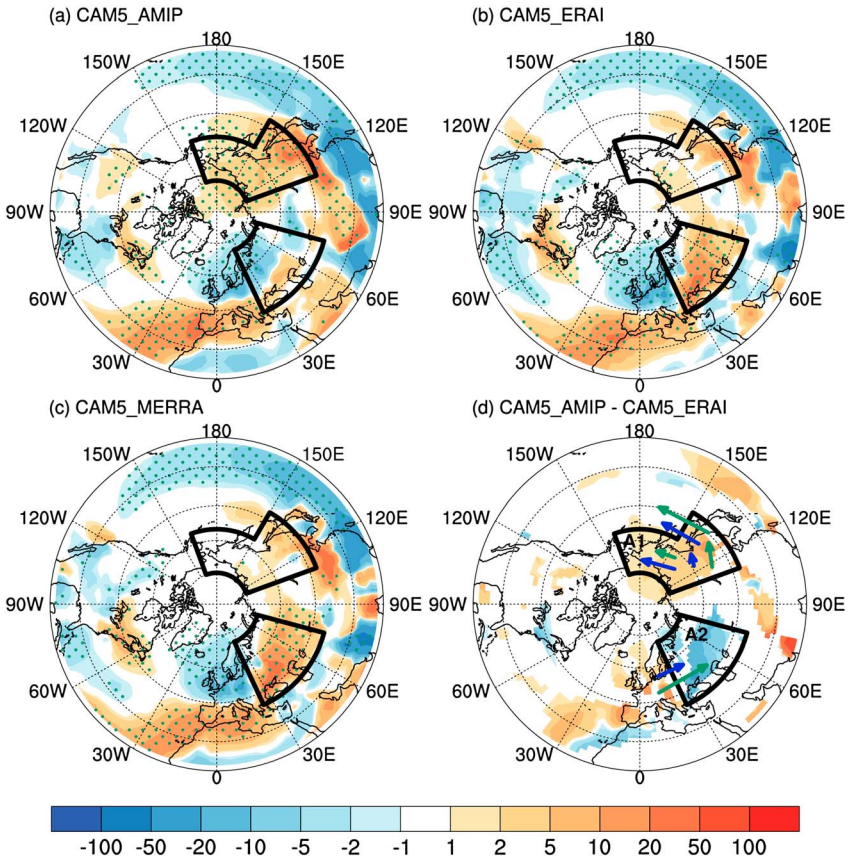

Figure 6. Lower tropospheric (below 688 hPa) BC burden regressed onto the AO index (color shaded; unit: μg m^{-2}) simulated by (a) CAM5_AMIP, (b) CAM5_ERAI, and (c) CAM5_MERRA, and (d) the difference of the regressed lower tropospheric BC burden between CAM5_AMIP and CAM5_ERAI when at least one of the regression coefficients is significant, with schematic air mass flux for CAM5_AMIP (blue arrow) and CAM5_ERAI (green arrow). Two areas of interest are marked as A1 and A2. Stippled area denotes the statistically significant regression with significance level = 0.05 using Student's *t* test.

transport than the GCM-driven simulation by about 50% (at a significance level of 0.05). The interannual variability of transient eddy transport is also larger in the reanalysis-driven experiments. The GCM-driven simulation shows a 20% larger stationary eddy transport than the reanalysis-driven simulations (statistically significance of 0.1).

[17] To further understand the difference of the lower tropospheric eddy transport between the GCM- and reanalysis-driven simulation, we computed the meridional component of the eddy kinetic energy (EKE), BC burden below 700 hPa, and meridional BC transport in the lower troposphere (below 700 hPa) over the eastern Atlantic/northern Europe region along 50°N–65°N averaged over 30°W–90°E, where most poleward BC transport takes place. Results from the two reanalysis-driven simulations are normalized with respect to the GCM-driven simulation, as shown in Figure 4.

[18] The EKE is about 30% higher in the two reanalysis data sets than the free-running simulation. Lower tropospheric BC burden in the reanalysis-driven simulations is about 10% lower than the GCM-driven experiment south of 60°N. Poleward BC transport is lower in the reanalysis-driven simulations but increases uniformly with latitude from 50°N to 65°N (seven latitudinal model grids) compared with the GCM-driven simulation. Poleward of 62°N, the two reanalysis-driven simulations show higher poleward BC transport, while the BC burdens are lower than the GCM-driven simulation. Thus, we conclude that the weaker poleward BC transport into the Arctic in CAM5_AMIP over the eastern Atlantic/northern Europe region is primarily due to its less efficient meridional transport of BC over the area as a result of fewer and weaker eddies. In other words, the GCM-driven simulation retains a larger portion of BC within the midlatitudes, and eventually, these particles are removed from the atmosphere.

3.3. Modulation of Meridional BC Transport Associated With the Arctic Oscillation

[19] Previous studies have found that the North Atlantic Oscillation (NAO) has a significant control over the transport of trace gases [*Burkhart et al.*, 2006; *Christoudias et al.*, 2012; *Creilson et al.*, 2003; *Eckhardt et al.*, 2003] and aerosols [*Gong et al.*, 2010; *Sharma et al.*, 2006] into the Arctic. In this study, we explore the dependence of BC transport on the Arctic Oscillation (AO), which is a close relative of the NAO and the dominant pattern of the variations of the mid- and high-latitude climates in the northern hemisphere [*Thompson and Wallace*, 1998]. The interannual variability of the BC transport into the Arctic modulated by AO in the GCM-driven simulation is evaluated against that in the two reanalysis-driven simulations.

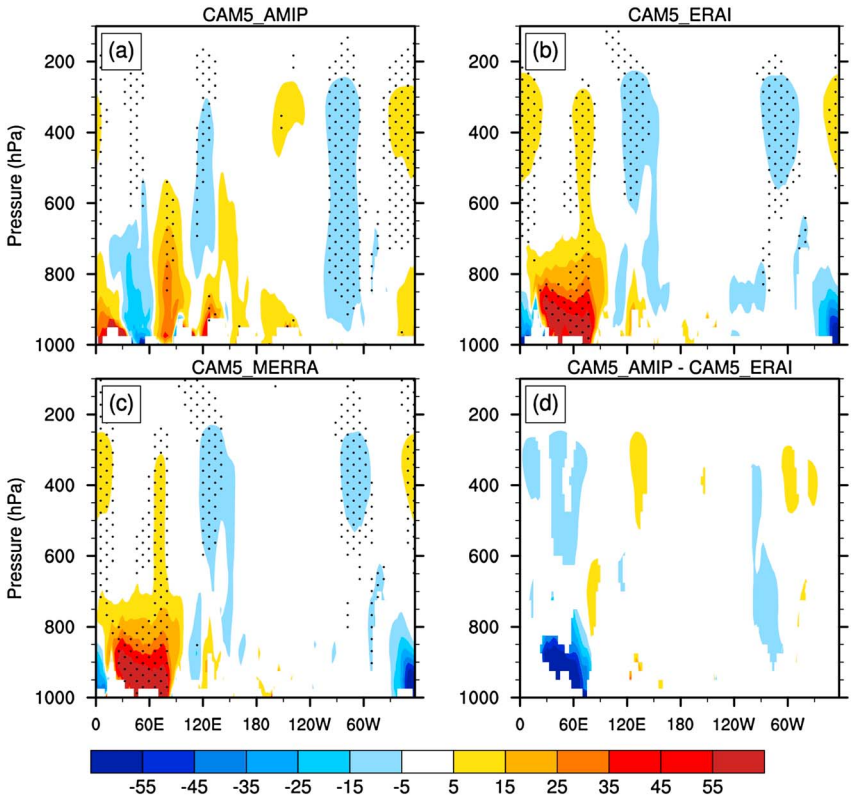

Figure 7. Cross-section of the difference of meridional BC flux (unit: ng m^{-2} s^{-1}) at 66.5°N between the positive and negative AO phase averaged over 22 years of DJF in (a) CAM5_AMIP, (b) CAM5_ERAI, and (c) CAM5_MERRA experiments, and (d) the difference between Figure 7a and Figure 7b when at least one of the meridional BC flux difference is significant. Stippled area denotes the statistically significant difference with significance level = 0.05 using Student's *t* test.

[20] We define the AO as the first empirical orthogonal function (EOF) of the 1000 hPa geopotential height (following the method suggested by the Climate Prediction Center of National Weather Service; http://www.cpc.ncep.noaa.gov/products/precip/CWlink/daily_ao_index/loading.html) over the 22 year simulation period. The Arctic region exhibits a relatively low pressure in the positive AO phase, and the pattern is reversed in the negative AO phase. As shown in Figures 5a–5c, the 22 year DJF mean circulation and the spatial pattern of the AO simulated in the GCM-driven simulation strongly resemble the prevailing winds and teleconnection patterns obtained from applying the identical calculation on the reanalysis data sets, ERA-Interim and MERRA. The explained variance of the first EOF and the temporal variability of the AO simulated in the free-running CAM5 defined as the variance of the first principle component (PC) are also about the same as the two reanalysis-driven experiments and are consistent with the findings in *Stoner et al.* [2009].

[21] Figure 5 also indicates some different characteristics of the simulated AO between the free-running CAM5 and reanalysis data sets. As also noted in *Stoner et al.* [2009] for different climate models, the GCM-simulated AO features a rotation about the polar region—both North Pacific and North Atlantic circulations are shifted westward by about 10–30°. The simulated variability of these two circulations is also different. During the positive AO phase, the GCM-simulated lower tropospheric westward (eastward) air mass flux anomalies over North Pacific Ocean (North Atlantic Ocean) are substantially stronger (weaker), suggesting much weaker (weaker) prevailing westerlies in the midlatitudes over East Asia and northwest Pacific Ocean (Europe) than the two reanalysis products.

[22] The differences in the simulated circulation anomalies can produce different BC transports associated with the AO. A correlation analysis shows that the AO index and the net meridional BC flux at 66.5°N are uncorrelated in the GCM-driven simulation (correlation coefficient $r = 0.06$) but well correlated in the reanalysis-driven simulations ($r = 0.57$). The area-mean wet removal rate between 30°N and 66.5°N is found to be uncorrelated with the AO index for all three experiments, suggesting that the interannual variability of net BC transport into the Arctic associated with the AO is dominated by the change of circulation, rather than the change of wet removal processes. A regression of the lower tropospheric BC burden onto the AO index for the three simulations (Figures 6a–6c) shows that while the GCM-driven simulation produces very similar BC distribution associated with the AO, large differences appear over northeast Asia (area A1 in Figure 6d) and eastern Europe (area A2 in Figure 6d). In the GCM-driven simulation, the weaker westerlies in midlatitudes over East Asia and northwest Pacific Ocean result in less zonal BC transport from East Asia to the Pacific Ocean, retaining BC in the source region. In comparison, the strong northeastward circulation anomaly produced over northeast Asia in CAM5_AMIP compared with CAM5_ERAI (Figure 5d) effectively

transports BC from Asian source regions to northeast Asia. These circulation biases cause the statistically significant increase of BC burden over area A1 during the positive AO phase. Over Europe, the GCM-simulated modulation of westerlies with the AO produces weaker westerlies, causing less BC transport from the western to eastern European region. Hence, the increase of lower tropospheric BC burden over area A2 is absent in the GCM-driven simulation (Figures 6a and 6d).

[23] The vertical structure of the poleward BC transport into the Arctic modulated by the AO (Figure 7) indicates an increased meridional BC flux in the middle and upper troposphere in the positive AO phase, associated with more efficient exchanges of air parcels. However, the northward and southward BC fluxes are weak and largely offset each other so that the net poleward BC transport in the middle and upper troposphere is insensitive to the AO.

[24] In the lower troposphere where most of the BC transport takes place (Table 2), the reanalysis-driven simulations show that poleward BC flux is shifted eastward by about 30° due to the modulation of westerlies with the AO (Figures 7b and 7c) and is significantly higher (significance level = 0.05) over eastern Europe and western Russia (30°E–90°E) in the positive AO phase as a result of higher BC burden transported from western Europe. However, in the GCM-driven simulation, because the circulation modulation associated with the AO over this region is primarily zonal, the variation of lower tropospheric meridional BC transport is generally weak or insignificant (Figure 7a). Over northeast Asia (120°E–150°E), the GCM-driven simulation produces a strong and significant enhancement of poleward BC transport in the positive AO phase (Figure 7a), corresponding to the northeastward circulation anomaly over this region (Figures 5a and 5d).

[25] Our analysis also shows that the poleward BC transport into the Arctic is concentrated over eastern Europe (30°E–90°E). The AO-modulated change of circulation produces a significant increase of poleward BC flux during the positive AO phase by about $50\,\mathrm{ng\,m^{-2}\,s^{-1}}$ (Figure 7), which is about a 50% variation from the mean poleward BC flux (Figure 2). The enhanced poleward BC transport suggests that the Arctic pollution can become more severe in the positive AO phase, which is consistent with previous studies [*Hurrell and VanLoon*, 1997; *Quinn et al*., 2007]. In the Arctic, the three off-line simulations show a stronger wet deposition in the Arctic during the positive AO phase (not shown), resulting in a strong positive correlation between the AO and Arctic BC deposition and a weak correlation between the AO and the atmospheric BC burden over the Arctic.

4. Conclusion

[26] Understanding the long-range transport of aerosols is a challenging task largely due to the complexity of processes that must be considered, including transport, removal, and the interactions between them. In this study, we explore the sensitivity of BC reaching the Arctic to circulation features important to transport. We have found that the mean circulation simulated by the free-running CAM5 is generally consistent with observed circulation features as represented in reanalysis products. Mean BC transport produced by circulations in the free-running simulation are quite similar to those produced by simulations constrained by observations via large-scale reanaylses. The large similarity suggests that much of the large underprediction of BC in the Arctic found in CAM5 is unlikely to be dominated by circulation biases, but must instead be assigned to the model treatment of other uncertain processes such as aerosol emissions and removal processes including the representation of cloud processing and aerosol-cloud interactions that occurs at subgrid scale.

[27] Although we attribute most of the biases in BC reaching the Arctic to cloud processes, there are some differences in transport characteristics found between the GCM- and reanalysis-driven simulations. The free-running CAM5 climate has fewer or weaker eddies, resulting in significantly weaker transient transport of BC from the source region to the high latitudes. This may be a consequence of the spatial resolution used in our GCM simulations. The current $1.9° \times 2.5°$ model resolution can only marginally represent the baroclinic eddies responsible for energy and tracer transport. Higher-resolution simulations are likely to produce a better simulation of those eddies and thereby enhance the eddy transport of aerosols (Appendix B). In the reanalysis products, the model fields were originally produced by higher-resolution simulations with high-frequency observations assimilated to retain realistic transient atmospheric motions. The dynamical features of the off-line simulations are thus treated more accurately with less opportunity for bias from numerical truncation issues or other factors leading to meteorological errors. Therefore, the fields used to drive the aerosol simulation from reanalysis products will be more realistic even though the aerosol simulations themselves were all run at the same spatial resolution. The resolution dependency of CAM5 physics and dynamics and its effect on BC transport into the Arctic will be documented in a separate paper.

[28] We also have found that while CAM5 is skillful in reproducing some of the teleconnection patterns in general, differences in the simulated spatial pattern of the AO result in different interannual variability of BC transport and burden associated with the AO, particularly over northeast Asia and eastern Europe, from those in simulations when the model's meteorology is constrained by observations. These differences are primarily due to the circulation biases in the model.

Appendix A: Model Evaluation

[29] The 22 year DJF mean latitudinal distribution is depicted in Figure A1. Driven by virtually the same meteorology, CAM5_AMIP greatly increases the lower tropospheric (below 3 km) BC burden by about 40%, while the total column BC burden increases only marginally compared with CAM5_AMIP_ORI. The GCM- and reanalysis-driven off-line simulations agree more on the latitudinal distribution of BC (Figures A1a–A1c), and less on dry and wet deposition in the midlatitudes (Figures A1d and A1e) due to the difference of the simulated surface winds stress and cloud fields. However, the removal rate in the three off-line simulations in the middle and high latitudes is almost identical (Figure A1f). In the Arctic, the two reanalysis-driven simulations show a 10–15% more BC deposition and similar (for CAM5_MERRA) or higher (for CAM5_ERAI) total column BC burden.

[30] Figure A2 compares simulated surface BC mixing ratio with in situ observations at Barrow (157°W, 71°N)

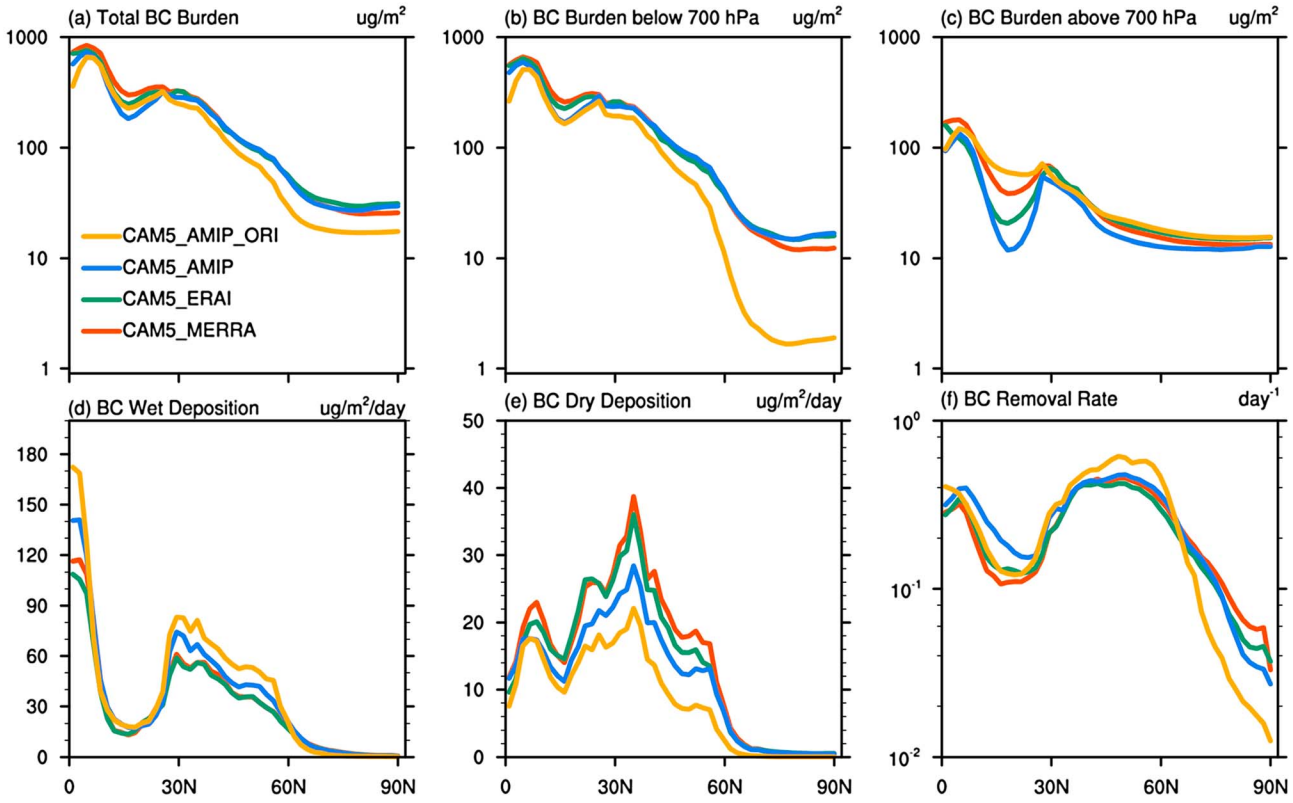

Figure A1. Zonal average (a) total column BC burden (unit = $\mu g\,m^{-2}$), (b) BC burden below 700 hPa (unit = $\mu g\,m^{-2}$), (c) BC burden above 700 hPa (unit = $\mu g\,m^{-2}$), (d) wet deposition of BC (unit = $\mu g\,m^{-2}\,day^{-1}$), (e) dry deposition of BC (unit = $\mu g\,m^{-2}\,day^{-1}$), and (f) BC removal rate (unit = day^{-1}), defined as the sum of BC dry and wet deposition, divided by total column BC burden. Results are averaged over 22 years of DJF.

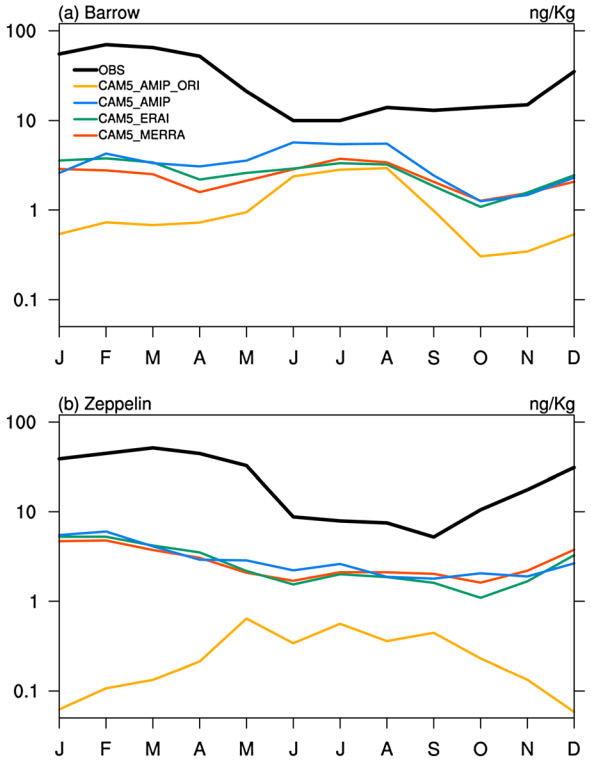

Figure A2. Time series of monthly average BC mixing ratio (unit = ng kg^{-1}) simulated by CAM5_AMIP_ORI (yellow), CAM5_AMIP (blue line), CAM5_ERAI (green), and CAM5_MERRA (red) compared with in situ observations (black) at (a) Barrow (157°W, 71°N) and (b) Zeppelin (12°E, 79°N). Model results are averaged over 22 years.

[*Sharma et al.*, 2006] and Zeppelin (12°E, 79°N) [*Eleftheriadis et al.*, 2009]. Comparing CAM5_AMIP_ORI and CAM5_AMIP shows a factor of 5 improvement of surface BC concentration over Barrow in the wintertime and about 2 orders of magnitude improvement over Zeppelin. However, overall, the model still greatly underpredicts BC by about a factor of 2 in the summer months and by 1 order of magnitude in the wintertime. In general, the difference between the three off-line experiments is small, especially in the wintertime. The similarity among the simulations suggests that the fidelity of the model wind fields and their transport aspects is very high.

[31] To evaluate the simulated vertical distribution of BC, we compared the simulated BC mixing ratio to aircraft measurements from the HIAPER Pole-to-Pole Observations campaign (HIPPO1) [*Schwarz et al.*, 2010], depicted in Figure A3. The results show an overall improvement of vertical distribution of BC when the model is implemented with the *Wang et al.* [2013] revised physics package. Over the west coast of the United States and the eastern Pacific Ocean (Figure A3b), the simulated BC agrees with the observations in the middle and high troposphere but overestimates lower tropospheric BC concentration (below 700 hPa). Nevertheless, around the same longitudes but at higher latitude, all model simulations underpredict BC below 500 hPa by about 1 order of magnitude (Figure A3a).

[32] In general, BC concentration at high latitudes increases significantly in the off-line simulations with the *Wang et al.* [2013] revised physics package. The remaining underestimation of surface BC concentration is not attributed to the circulation simulated by the model, since the GCM- and reanalysis-driven simulations render very similar BC transport and distribution.

Appendix B: Resolution Dependence

[33] The CESM1.0.3 supports two scientifically validated resolutions for the standalone CAM5 running in accordance with the AMIP protocol [*Gates et al.*, 1999] for the finite volume dynamical core [*Lin and Rood*, 1996, 1997]: the 1.9 × 2.5 (“2°”) and the 0.9 × 1.25 (“1°”) latitude-longitude grid spacings. To explore the sensitivity of BC transport into the Arctic to model resolution, we performed a pair of 4 year simulations for these two resolutions running with the standard CAM5 physics package.

[34] In Table B1, the results show that the transient eddy transport is the dominant term for BC transport into the Arctic for both simulations. With higher resolution, the model produces about 60% higher poleward eddy transport of BC into

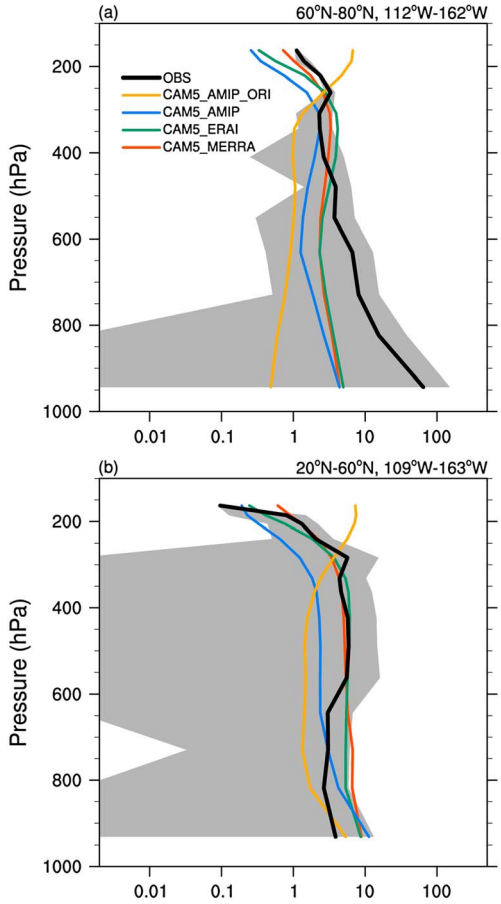

Figure A3. Vertical profile of monthly average BC mixing ratio (unit = ng kg^{-1}) simulated by CAM5_AMIP_ORI (yellow), CAM5_AMIP (blue), CAM5_ERAI (green), and CAM5_MERRA (red) in January 2009, evaluated against HIPPO1 aircraft measurements (black) in (a) high latitudes and (b) midlatitudes. Gray shaded area represents variability of the observational data within one standard deviation from the mean.

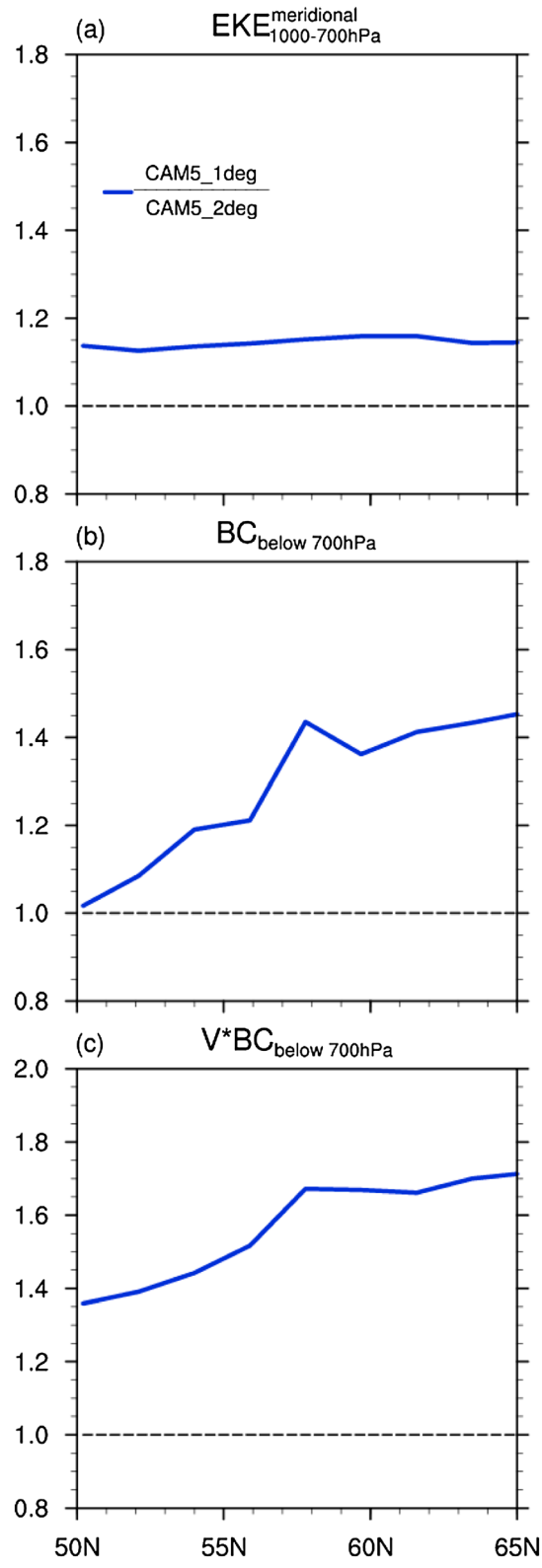

Figure B1. Lower tropospheric (a) eddy kinetic energy, (b) BC burden, and (c) meridional BC flux of the 1° resolution simulation in DJF as a function of latitude, averaged over eastern Atlantic/northern Europe region (30°W–90°E) and normalized with respect to the 2° resolution simulation. Dashed line represents the 1:1 ratio.

Table B1. Net Meridional BC Flux (Unit = μg s^{-1} m^{-1}) Across 66.5°N in DJF, Averaged Over 4 Years

	1°	2°
Mean circulation transport	1.01	0.52
Stationary eddy transport	6.09	3.49
Transient eddy transport	10.34	6.56

the Arctic. For eastern Atlantic/northern Europe region (30°W–90°E) where most of the poleward BC transport takes place, Figure B1 shows that the 1° model simulation better resolves the synoptic scale eddies, producing the EKE 15% higher than that in the 2° simulation across the domain. Consequently, the poleward BC transport (Figure B1c) increases significantly from 50°N to 65°N, contributing to about 60% higher BC transport into the Arctic.

[35] **Acknowledgments.** The ERA-Interim data are obtained from Research Data Archive (RDA) which is maintained by the Computational and Information Systems Laboratory (CISL) at the National Center for Atmospheric Research (NCAR). NCAR is sponsored by the National Science Foundation (NSF). The MISR AOT data used in this study are obtained from the Giovanni online data system, developed and maintained by the NASA GES DISC. This study is supported by the Office of Science (BER), U.S. Department of Energy. The Pacific Northwest National Laboratory is operated for DOE by Battelle Memorial Institute under contract DE-AC06-76RLO 1830.

References

Bey, I., D. J. Jacob, R. M. Yantosca, J. A. Logan, B. D. Field, A. M. Fiore, Q. B. Li, H. G. Y. Liu, L. J. Mickley, and M. G. Schultz (2001), Global modeling of tropospheric chemistry with assimilated meteorology: Model description and evaluation, *J. Geophys. Res.*, *106*(D19), 23,073–23,095.

Bond, T. C., D. G. Streets, K. F. Yarber, S. M. Nelson, J. H. Woo, and Z. Klimont (2004), A technology-based global inventory of black and organic carbon emissions from combustion, *J. Geophys. Res.*, *109*, D14203, doi:10.1029/2003JD003697.

Bond, T. C., et al. (2013), Bounding the role of black carbon in the climate system: A scientific assessment. *J. Geophys. Res.*, *118*, doi:10.1002/jgrd.50171.

Bony, S., M. J. Webb, C. S. Bretherton, S. A. Klein, A. P. Siebesma, G. Tselioudis, and M. Zhang (2011), CFMIP: Towards a better evaluation and understanding of clouds and cloud feedbacks in CMIP5 models, *CLIVAR Exchanges*, *16*(56), 20–24.

Burkhart, J. F., R. C. Bales, J. R. McConnell, and M. A. Hutterli (2006), Influence of North Atlantic Oscillation on anthropogenic transport recorded in northwest Greenland ice cores, *J. Geophys. Res.*, *111*, D22309, doi:10.1029/2005JD006771.

Chepfer, H., S. Bony, D. Winker, M. Chiriaco, J. L. Dufresne, and G. Seze (2008), Use of CALIPSO lidar observations to evaluate the cloudiness simulated by a climate model, *Geophys. Res. Lett.*, *35*, L15704, doi:10.1029/2008GL034207 .

Chepfer, H., S. Bony, D. Winker, G. Cesana, J. L. Dufresne, P. Minnis, C. J. Stubenrauch, and S. Zeng (2010), The GCM-Oriented CALIPSO Cloud Product (CALIPSO-GOCCP), *J. Geophys. Res.*, *115*, D00H16, doi:10.1029/2009JD012251.

Chin, M., R. B. Rood, S. J. Lin, J. F. Muller, and A. M. Thompson (2000), Atmospheric sulfur cycle simulated in the global model GOCART: Model description and global properties, *J. Geophys. Res.*, *105*(D20), 24,671–24,687.

Chipperfield, M. P. (2006), New version of the TOMCAT/SLIMCAT off-line chemical transport model: Intercomparison of stratospheric tracer experiments, *Q. J. R. Meteorol. Soc.*, *132*(617), 1179–1203.

Christoudias, T., A. Pozzer, and J. Lelieveld (2012), Influence of the North Atlantic Oscillation on air pollution transport, *Atmos. Chem. Phys.*, *12*(2), 869–877.

Creilson, J. K., J. Fishman, and A. E. Wozniak (2003), Intercontinental transport of tropospheric ozone: A study of its seasonal variability across the North Atlantic utilizing tropospheric ozone residuals and its relationship to the North Atlantic Oscillation, *Atmos. Chem. Phys.*, *3*, 2053–2066.

Dee, D. P., et al. (2011), The ERA-Interim reanalysis: Configuration and performance of the data assimilation system, *Q. J. R. Meteorol. Soc.*, *137*(656), 553–597.

Eckhardt, S., A. Stohl, S. Beirle, N. Spichtinger, P. James, C. Forster, C. Junker, T. Wagner, U. Platt, and S. G. Jennings (2003), The North

Atlantic Oscillation controls air pollution transport to the Arctic, *Atmos. Chem. Phys.*, *3*, 1769–1778.

Eleftheriadis, K., S. Vratolis, and S. Nyeki (2009), Aerosol black carbon in the European Arctic: Measurements at Zeppelin station, Ny-Alesund, Svalbard from 1998–2007, *Geophys. Res. Lett.*, *36*, L02809, doi:10.1029/2008GL035741.

Emmons, L. K., et al. (2010), Description and evaluation of the Model for Ozone and Related chemical Tracers, version 4 (MOZART-4), *Geosci. Model Dev.*, *3*(1), 43–67.

Fisher, J. A., et al. (2010), Source attribution and interannual variability of Arctic pollution in spring constrained by aircraft (ARCTAS, ARCPAC) and satellite (AIRS) observations of carbon monoxide, *Atmos. Chem. Phys.*, *10*(3), 977–996.

Flanner, M. G., C. S. Zender, J. T. Randerson, and P. J. Rasch (2007), Present-day climate forcing and response from black carbon in snow, *J. Geophys. Res.*, *112*, D11202, doi:10.1029/2006JD008003.

Flanner, M. G., C. S. Zender, P. G. Hess, N. M. Mahowald, T. H. Painter, V. Ramanathan, and P. J. Rasch (2009), Springtime warming and reduced snow cover from carbonaceous particles, *Atmos. Chem. Phys.*, *9*(7), 2481–2497.

Gates, W. L., et al. (1999), An overview of the results of the Atmospheric Model Intercomparison Project (AMIP I), *Bull. Am. Meteorol. Soc.*, *80*(1), 29–55.

Ginoux, P., M. Chin, I. Tegen, J. M. Prospero, B. Holben, O. Dubovik, and S. J. Lin (2001), Sources and distributions of dust aerosols simulated with the GOCART model, *J. Geophys. Res.*, *106*(D17), 20,255–20,273.

Gong, S. L., T. L. Zhao, S. Sharma, D. Toom-Sauntry, D. Lavoue, X. B. Zhang, W. R. Leaitch, and L. A. Barrie (2010), Identification of trends and interannual variability of sulfate and black carbon in the Canadian High Arctic: 1981-2007, *J. Geophys. Res.*, *115*, D07305, doi:10.1029/2009JD012943.

Hansen, J., and L. Nazarenko (2004), Soot climate forcing via snow and ice albedos, *Proc. Natl. Acad. Sci. U. S. A.*, *101*(2), 423–428.

Heimann, M. (1995), The Global Atmospheric Tracer Model TM2, *Tech. Rep. 10*, Hamburg, Germany.

Huang, L., S. L. Gong, S. Sharma, D. Lavoue, and C. Q. Jia (2010), A trajectory analysis of atmospheric transport of black carbon aerosols to Canadian high Arctic in winter and spring (1990-2005), *Atmos. Chem. Phys.*, *10*(11), 5065–5073.

Hurrell, J. W., and H. VanLoon (1997), Decadal variations in climate associated with the north Atlantic oscillation, *Clim. Change*, *36*(3-4), 301–326.

Jacob, D. J., et al. (1997), Evaluation and intercomparison of global atmospheric transport models using Rn-222 and other short-lived tracers, *J. Geophys. Res.*, *102*(D5), 5953–5970.

Kahn, R. A., B. J. Gaitley, M. J. Garay, D. J. Diner, T. F. Eck, A. Smirnov, and B. N. Holben (2010), Multiangle Imaging SpectroRadiometer global aerosol product assessment by comparison with the Aerosol Robotic Network, *J. Geophys. Res.*, *115*, D23209, doi:10.1029/2010JD014601.

Kay, J. E., et al. (2012), Exposing global cloud biases in the Community Atmosphere Model (CAM) using satellite observations and their corresponding instrument simulators, *J. Clim.*, *25*(15), 5190–5207.

Koch, D., and J. Hansen (2005), Distant origins of Arctic black carbon: A Goddard Institute for Space Studies ModelE experiment, *J. Geophys. Res.*, *110*, D04204, doi:10.1029/2004JD005296.

Koch, D., et al. (2009), Evaluation of black carbon estimations in global aerosol models, *Atmos. Chem. Phys.*, *9*(22), 9001–9026.

von Kuhlmann, R., M. G. Lawrence, P. J. Crutzen, and P. J. Rasch (2003a), A model for studies of tropospheric ozone and nonmethane hydrocarbons: Model evaluation of ozone-related species, *J. Geophys. Res.*, *108*(D23), 4729, doi:10.1029/2002JD003348.

von Kuhlmann, R., M. G. Lawrence, P. J. Crutzen, and P. J. Rasch (2003b), A model for studies of tropospheric ozone and nonmethane hydrocarbons: Model description and ozone results, *J. Geophys. Res.*, *108*(D9), 4294, doi: 10.1029/2002JD002893.

Lamarque, J. F., et al. (2010), Historical (1850–2000) gridded anthropogenic and biomass burning emissions of reactive gases and aerosols: Methodology and application, *Atmos. Chem. Phys.*, *10*(15), 7017–7039.

Lamarque, J. F., et al. (2012), CAM-chem: Description and evaluation of interactive atmospheric chemistry in the Community Earth System Model, *Geosci. Model Dev.*, *5*(2), 369–411.

Law, K. S., and A. Stohl (2007), Arctic air pollution: Origins and impacts, *Science*, *315*(5818), 1537–1540.

Lawrence, M. G., P. J. Crutzen, P. J. Rasch, B. E. Eaton, and N. M. Mahowald (1999), A model for studies of tropospheric photochemistry: Description, global distributions, and evaluation, *J. Geophys. Res.*, *104*(D21), 26245–26277.

Lee, Y. H., et al. (2012), Evaluation of preindustrial to present-day black carbon and its albedo forcing from ACCMIP (Atmospheric Chemistry and Climate Model Intercomparison Project), *Atmos. Chem. Phys. Discuss.*, *12*(8), 21713–21778.

Lin, S. J., and R. B. Rood (1996), Multidimensional flux-form semi-Lagrangian transport schemes, *Mon. Weather Rev.*, *124*(9), 2046–2070.

Lin, S. J., and R. B. Rood (1997), An explicit flux-form semi-Lagrangian shallow-water model on the sphere, *Q. J. R. Meteorol. Soc.*, *123*(544), 2477–2498.

Liu, J. F., S. M. Fan, L. W. Horowitz, and H. Levy (2011), Evaluation of factors controlling long-range transport of black carbon to the Arctic, *J. Geophys. Res.*, *116*, D04307, doi:10.1029/2010JD015145.

Liu, X., et al. (2012), Toward a minimal representation of aerosols in climate models: Description and evaluation in the Community Atmosphere Model CAM5, *Geosci. Model Dev.*, *5*(3), 709–739.

Neale, R. B., et al. (2010), Description of the NCAR Community Atmosphere Model (CAM5), *Technical Report NCAR/TN-486+STR*, 268 pp, National Center for Atmospheric Research, Boulder, Colo.

Quinn, P. K., G. Shaw, E. Andrews, E. G. Dutton, T. Ruoho-Airola, and S. L. Gong (2007), Arctic haze: Current trends and knowledge gaps, *Tellus, Ser. B*, *59*(1), 99–114.

Ramanathan, V., and G. Carmichael (2008), Global and regional climate changes due to black carbon, *Nat. Geosci.*, *1*(4), 221–227.

Rasch, P. J., N. M. Mahowald, and B. E. Eaton (1997), Representations of transport, convection, and the hydrologic cycle in chemical transport models: Implications for the modeling of short-lived and soluble species, *J. Geophys. Res.*, *102*(D23), 28,127–28,138.

Rasch, P. J., et al. (2000), A comparison of scavenging and deposition processes in global models: Results from the WCRP Cambridge Workshop of 1995, *Tellus, Ser. B*, *52*(4), 1025–1056.

Rienecker, M. M., et al. (2011), MERRA: NASA's Modern-Era Retrospective Analysis for Research and Applications, *J. Clim.*, *24*(14), 3624–3648.

Schwarz, J. P., J. R. Spackman, R. S. Gao, L. A. Watts, P. Stier, M. Schulz, S. M. Davis, S. C. Wofsy, and D. W. Fahey (2010), Global-scale black carbon profiles observed in the remote atmosphere and compared to models, *Geophys. Res. Lett.*, *37*, L18812, doi:10.1029/2010GL044372.

Sharma, S., E. Andrews, L. A. Barrie, J. A. Ogren, and D. Lavoue (2006), Variations and sources of the equivalent black carbon in the high Arctic revealed by long-term observations at Alert and Barrow: 1989-2003, *J. Geophys. Res.*, *111*, D14208, doi:10.1029/2005JD006581.

Shindell, D. T., et al. (2008), A multi-model assessment of pollution transport to the Arctic, *Atmos. Chem. Phys.*, *8*(17), 5353–5372.

Stohl, A. (2006), Characteristics of atmospheric transport into the Arctic troposphere, *J. Geophys. Res.*, *111*, D11306, doi:10.1029/2005JD006888.

Stoner, A. M. K., K. Hayhoe, and D. J. Wuebbles (2009), Assessing general circulation model simulations of atmospheric teleconnection patterns, *J. Clim.*, *22*(16), 4348–4372.

Textor, C., et al. (2006), Analysis and quantification of the diversities of aerosol life cycles within AeroCom, *Atmos. Chem. Phys.*, *6*, 1777–1813.

Thompson, D. W. J., and J. M. Wallace (1998), The Arctic Oscillation signature in the wintertime geopotential height and temperature fields, *Geophys. Res. Lett.*, *25*(9), 1297–1300.

Vavrus, S., and D. Waliser (2008), An improved parametrization for simulating Arctic cloud amount in the CCSM3 climate model, *J. Clim.*, *21*(21), 5673–5687.

Wang, M., et al. (2011a), The multi-scale aerosol-climate model PNNL-MMF: Model description and evaluation, *Geosci. Model Dev.*, *4*(1), 137–168.

Wang, Q., et al. (2011b), Sources of carbonaceous aerosols and deposited black carbon in the Arctic in winter-spring: Implications for radiative forcing, *Atmos. Chem. Phys.*, *11*(23), 12453–12473.

Wang, H., R. C. Easter, P. J. Rasch, M. Wang, X. Liu, S. J. Ghan, Y. Qian, J. H. Yoon, P. L. Ma, and V. Velu (2013), Sensitivity of remote aerosol distributions to representation of cloud-aerosol interactions in a global climate model, *Geosci. Model Dev. Discuss.*, *6*(1), 331–378.